NUMERICAL AND EXPERIMENTAL STUDY OF LOCAL RESIN PRESSURE FOR THE MANUFACTURING OF COMPOSITE STRUCTURES AND THEIR EFFECT ON POROSITY

Houman Bedayat[1], Alireza Forghani[1], Curtis Hickmott[1], Frank Palmieri[2], Brian Grimsley[2], Brian Coxon[1], Goran Fernlund[1,3] Anoush Poursartip[1,3]

[1] Convergent Manufacturing Technologies US, Seattle, WA
[2] NASA Langley Research Center, Hampton, VA
[3] Department of Materials Engineering, The University of British Columbia, Vancouver, BC, Canada

ABSTRACT

Porosity can have significant impact on the mechanical performance of composite structures. The primary sources of voids during the cure of composites include air entrapped during lay-up, bag or tool leaks, and the off gassing of volatiles. Capturing the physics of void evolution during composite processing is a challenge due to the number of sources and changing phenomena that give rise to voids as the resin cures. Local changes in resin pressure due to geometric features or cure shrinkage have been experimentally linked to a higher likelihood of void formation. In this work, a preliminary model was developed to predict local resin pressure which can be used to identify regions more susceptible to porosity. Experiments were conducted to validate the model accuracy. Ultimately, this model can be used as a tool to minimize the likelihood of porosity by optimizing the material selection, part design, layup, and cure process.

1. INTRODUCTION

Porosity, as a manufacturing process-induced defect, highly affects the mechanical properties of cured composites. There are several contributing factors to the formation of porosity in composite structures, most notably air entrapped during lay-up, bag or tool leaks, and the off gassing of volatiles. The variety of factors that cause porosity highlights the multi-scale and multi-physics nature of porosity formation and presents a challenging problem. Understanding how these mechanisms contribute to the formation of porosity is a key component of minimizing their negative effect [1].

Experimental evidence shows that local resin pressure history plays a major role in void growth during a cure cycle [2]. Therefore, the prediction of local resin pressure has been the focus of modeling the porosity in composite structures. The goal of this study is to develop and validate a model for formation of porosity during the cure process of complex composite structures. This research focuses on formation of voids using an epoxy carbon fiber prepreg that was fabricated via hand lay-up and cured in an autoclave.

1.1 Prepreg manufacturing process

Thermoset prepreg is a form of raw composite material in which the fibers (woven or uni-directional) are pre-impregnated with an uncured thermoset resin which will cure at elevated temperatures. In composite manufacturing, the composite part is made by deposition of prepreg plies

on a tool (lay-up). After lay-up and bagging, the part is processed under a defined temperature and pressure cycle. Compaction pressure, i.e. the pressure difference between the interior and exterior of the vacuum bag, and temperature are two important processing parameters which control the part consolidation, cure, and final quality. Compaction pressure creates the driving force for fiber bed compaction and resin flow during processing whereas vacuum pressure aids with gas removal and porosity reduction throughout the process [3]. In turn, the temperature history determines the degree of cure, and the viscosity of the resin is a function of the degree of cure.

Porosity formation occurs nearly throughout the entire process cycle. In Figure 1, a representative process cycle is shown divided into distinct stages.

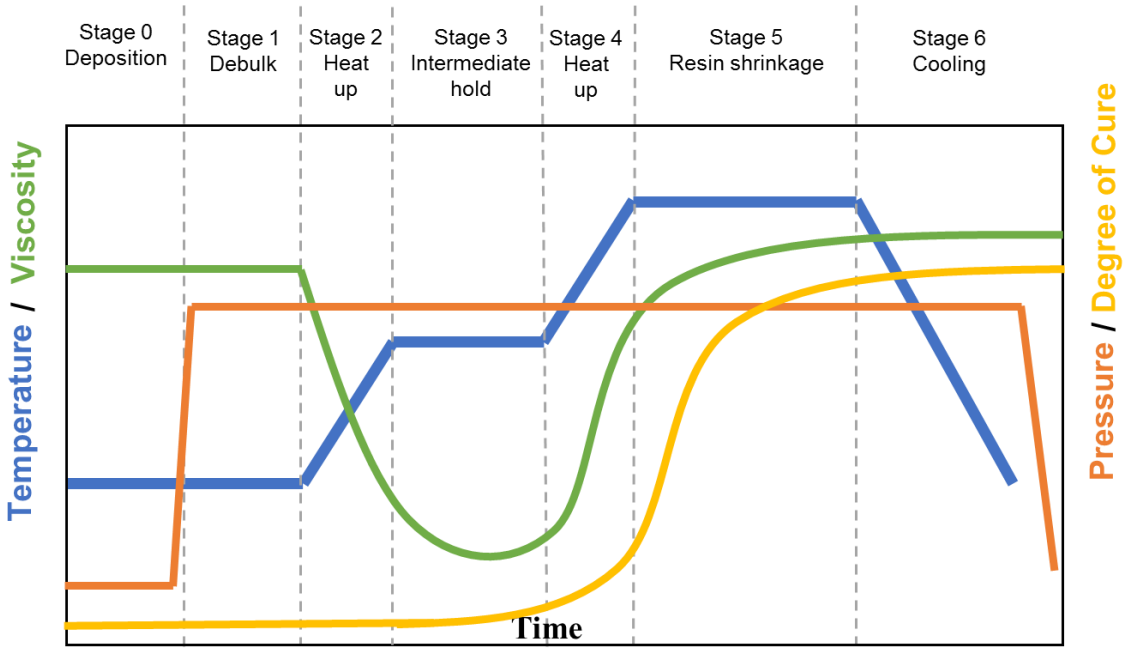

Figure 1. Schematic of the stages in an autoclave process cycle, modified from Bedayat et al. [1]

At stage 0 (deposition), the primary source of porosity is entrapped air between the plies. As the material debulks (stage 1), the part thickness is reduced, but some air may remain entrapped if there are no continuous evacuation paths to the vacuum system. When the temperature elevates in stage 2 (heat up), the reduction in viscosity causes gas evacuation pathways to collapse. Holding the temperature at stage 3 (intermediate hold) helps to remove moisture and volatiles from the system and consolidate the plies. Further increase in the temperature profile at stage 4 (second heat up) leads to an increase in vapor pressure of the moisture and volatiles in the resin resulting in off-gassing or diffusion of volatiles from the resin to existing gas bubbles. By stage 5 (resin shrinkage), most of the resin has already crosslinked, and material shrinkage has occurred. The remaining voids become locked in the material, and are the precursors to the final porosity in the cured part. Finally, at stage 6 (cooling), the voids in the resin have become locked into the part as final porosity. Any volatiles that remain in solution no longer influence the porosity of the vitrified matrix resin.

1.2 Modeling Framework

Multiple phenomena affect the formation of porosity during the cure process. A thorough porosity model should be able to cover void shrinkage and collapse, and gas and resin flow into void space. Our suggested physics-based model covers Mass Conservation for Three Phases (Fiber, Resin, and Gas), Fluid Flow Models (Resin and Gas), Fluid Pressure Equations, and Equilibrium Equation.

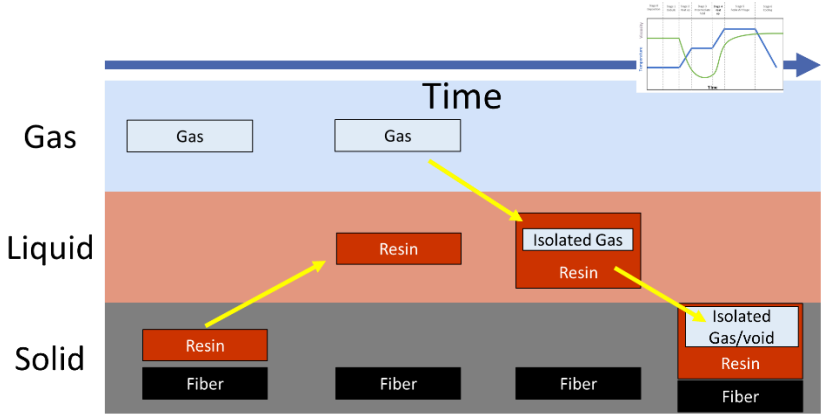

Figure 2: Schematic of different material phases during the cure process.

In uncured fiber-reinforced composites (e.g. prepreg system), the interaction of uncured liquid resin (moving fluid) in a fiber-bed structure (porous structure) determines the mechanical response of the medium. This phenomenon becomes more complex when more than one fluid (for example, gas in the composite manufacturing process) exists in the medium.

1.2.1 Governing Equations (IFS3P)

Poroelasticity is the science of describing the flow, stress and deformation mechanisms in porous media and was originally developed in the field of soil mechanics [4]–[7]. The recent research performed at The University of British Columbia (described below) has extended poroelasticity concepts and methodology to simulation of cure processes in composites.

The composite manufacturing process involves resin and gas flow through the fiber-bed, thermochemical changes and phase transformations during resin cure, and a build-up of residual stress and dimensional variations in the final part [8]. Building off earlier work by Hubert ([9]-[10]), Haghshenas [11] focused on the composite manufacturing process, and developed a framework that integrated both resin and stress development into a unified process model for composite materials. Using classical flow through porous media models [5], [7], [12], Haghshenas created an Integrated Flow Stress (IFS) model enabling a seamless connection to the regime of the process simulation. This IFS model was successfully applied to case studies when typical boundary conditions were considered.

Based on Haghshenas [11], Niaki et al. [13] upgraded the models for the general case of a resin-fiber composite material system that, as a consequence of curing, undergoes a transition from a fluid-like state into an elastic solid. The constitutive equations employed in these models provide a continuous representation of the evolving material behavior while maintaining consistency with the formulations that are typically used to represent the material at each of the two extremes. Later, Niaki et al. [14] added the second fluid phase (gas) equations to the framework, presented in Equations (1)-(5) and briefly reviewed below.

The IFS3P mass conservation equation is as follows [8]

$$b\,\dot{u}_{i,i} + v_{F\,i,i} + v_{\hat{F}\,i,i} + \frac{b-\phi}{K_s}\dot{\psi}_F\,P_F + \frac{b-\phi}{K_s}\dot{\psi}_{\hat{F}}\,P_{\hat{F}} + \left(\frac{\phi_F}{K_F} + \frac{\psi_F(b-\phi)}{K_s}\right)\dot{P}_F + \left(\frac{\phi_{\hat{F}}}{K_{\hat{F}}} + \frac{\psi_{\hat{F}}(b-\phi)}{K_s}\right)\dot{P}_{\hat{F}} - \psi_F(1-\lambda)\delta_{ij}\,\dot{\varepsilon}^f_{F\,ij} - \psi_{\hat{F}}\delta_{ij}\,\dot{\varepsilon}^f_{\hat{F}\,ij} + (1-\phi)(1-\lambda)\,\delta_{ij}\dot{\varepsilon}^f_{S\,ij} - \frac{1}{3K_s}\delta_{ij}D_{SK_{ijkl}}\,\dot{\varepsilon}^f_{SK\,kl} = 0 \qquad (1)$$

where the subscripts F and $\hat{F}$ denote the corresponding parameters for resin and gas phases and subscripts S and SK denote the corresponding parameters for fibers (solid) and fiber-bed structure (solid skeleton) in the system. In Equation (1), u is displacement of the fiber bed structure, v is the volume-averaged relative velocity (Darcy velocity) of the fluid phases, P is pore fluid pressure, K is bulk moduli, ϕ is the volume fraction of the fluid phase, ψ is degree of saturation of each fluid phase, and ε^f is free strain. λ is a measure of the solidification of the fluid phase and varies between zero and unity, $0 \le \lambda \le 1$ ($\lambda = 0$ corresponds to the unsolidified fluid resin and $\lambda = 1$ corresponds to the fully solidified resin). The Darcy equation is used for flow of each of the fluid phases as follows

$$P_{F\,i} + \mu_F S_F^{-1}{}_{ij} v_{F\,j} = 0 \qquad (2)$$

$$P_{\hat{F}\,i} + \mu_{\hat{F}} S_{\hat{F}}^{-1}{}_{ij} v_{\hat{F}\,j} = 0 \qquad (3)$$

where μ is the fluid viscosity, and S_{ij} is the permeability tensor of the solid skeleton which is an average representation (or effective property) of the porous medium.

Finally, the equilibrium equation is written as

$$\sigma_{SK\,ij,j} - b\left(\psi_F\,P_{F,i} + \psi_{\hat{F}}\,P_{\hat{F},i}\right) = 0 \qquad (4)$$

where

$$\dot{\sigma}_{SK\,ij} = D_{SK_{ijkl}}\left(\frac{1}{2}\left(\dot{u}_{k,l} + \dot{u}_{l,k}\right) - \dot{\varepsilon}^f_{SK\,kl}\right) + \dot{b}\left(\psi_F\,P_{F,i} + \psi_{\hat{F}}\,P_{\hat{F},i}\right)\delta_{ij} \qquad (5)$$

1.2.2 Simplified model (IFS3P*)

Since commercially available Finite Element Analysis (FEA) solvers do not provide the means of simulating two independent Darcy flows, the above governing equations cannot be simulated. As a first approach to overcome this issue, it was assumed that resin and gas phases experience the same pressure. This was a reasonable assumption when the resin viscosity was low in the pre-gelation regime. Given this assumption, the governing equations will reduce into the following equations expressed in terms of an equivalent hybrid fluid ($\bar{F}$).

For mass conservation, Equation (1) simplifies to

$$b\,\dot{u}_{i,i} + v_{\bar{F}\,i,i} + \left(\frac{\phi_{\bar{F}}}{K_{\bar{F}}} + \frac{(b-\phi)}{K_s}\right)\dot{P}_{\bar{F}} - \phi_{\bar{F}}\dot{\varepsilon}^f_{\bar{F}\,ij} + (1-\phi)(1-\lambda)\,\delta_{ij}\dot{\varepsilon}^f_{S\,ij} - \frac{1}{3K_s}\delta_{ij}D_{SK_{ijkl}}\,\dot{\varepsilon}^f_{SK\,kl} = 0 \qquad (6)$$

where

$$v_{\bar{F}_{i,i}} = \psi_F v_{F_{i,i}} + \psi_{\hat{F}} v_{\hat{F}_{i,i}} \tag{7}$$

$$\frac{\phi_{\bar{F}}}{K_{\bar{F}}} = \frac{\phi_F}{K_F} + \frac{\phi_{\hat{F}}}{K_{\hat{F}}} \tag{8}$$

$$\phi_{\bar{F}} \dot{\varepsilon}^f_{\bar{F}_{ij}} = \psi_F (1-\lambda) \delta_{ij} \dot{\varepsilon}^f_{F_{ij}} - \psi_{\hat{F}} \delta_{ij} \dot{\varepsilon}^f_{\hat{F}_{ij}} \tag{9}$$

Similarly, the Darcy equation for fluid flow (Equations (2) and (3)) simplify to

$$P_{\bar{F}_i} + \mu_{\bar{F}} S^{-1}_{\bar{F}_{ij}} v_{\bar{F}_j} = 0 \tag{10}$$

where

$$\mu_{\bar{F}} S^{-1}_{\bar{F}_{ij}} v_{\bar{F}_j} = \psi_F \mu_F S^{-1}_{F_{ij}} v_{F_j} + \psi_{\hat{F}} \mu_{\hat{F}} S^{-1}_{\hat{F}_{ij}} v_{\hat{F}_j} \tag{11}$$

And the equilibrium equation (Equations (4) and (5)) become

$$\sigma_{SK_{ij,j}} - b P_{\bar{F},i} = 0 \tag{12}$$

where

$$\dot{\sigma}_{SK_{ij}} = D_{SK_{ijkl}} \left(\frac{1}{2} \left(\dot{u}_{k,l} + \dot{u}_{l,k} \right) - \dot{\varepsilon}^f_{SK_{kl}} \right) + \dot{b} P_{\bar{F},i} \delta_{ij} \tag{13}$$

By writing the governing equations in terms of the equivalent hybrid fluid ($\bar{F}$), it was possible to use available commercial FEA solvers for numerical simulations. Finite Element simulations presented here were performed using COMPRO implemented in ANSYS [15]. Convergent's COMPRO simulation software is a plug-in for general purpose FEA solvers designed for advanced simulation and process analysis of geometrically complex structures. Capabilities include thermal profiling and process design, porosity assessment and mitigation, and warpage and spring-back predictions.

2. EXPERIMENTATION

2.1 Local Resin Pressure Tests Methods

In order to evaluate the proposed modeling framework, a series of tests, similar to research performed at The University of British Columbia [2], [16], were developed to interrogate the local resin pressure response under a variety of conditions. A composite laminate was designed with symmetric ply drop along the length as shown in Figure 3, after the work described in [16]. This configuration creates pressure gradients promoting the flow of resin along the length of the ply drops, creating low pressure regions more susceptible to void formation. The primary variables of interest included ply drop offs (tapered geometry), caul sheet stiffness, fiber orientation and laminate thickness. The material used in this study was Hexcel IM7/8552-1 prepreg.

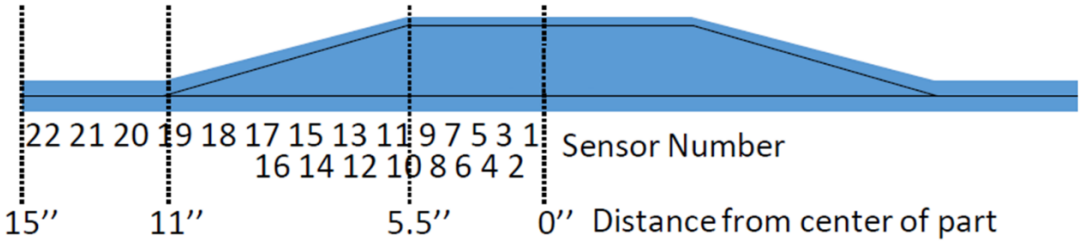

Figure 3: Schematic of laminate and caul sheet.

A tool was instrumented with resin pressure sensors along the length of the ply drops to measure the local resin pressure in the laminate. The location of the sensors in the tool is shown in Figure 4 and the panel configurations are shown in Table 1. Each variable in the test matrix influences the resin flow and local resin pressure enough to cause changes to the resin pressure history and void evolution, so that the trends observed can be used to validate the proposed model structure. The test plan is shown below in Table 1, and the corresponding cure cycle for these panels is shown below. Ply drops have been chosen in combination with variation in caul sheet weight and stiffness to drive resin flow by creating a pressure gradient from the thick region of the laminate towards the thin region. Three caul sheet configurations have been chosen; a stiff caul (0.5 in, 12.7mm), a flexible caul (0.125 in, 3.175 mm) and no caul (vacuum bag only). In each design, the imposed pressure gradient should vary enough to enable measurement with the sensors distributed in the tooling. The caul sheets in all three cases are made of aluminum. Two fiber orientations have been studied, a quasi-isotropic panel and a unidirectional panel with the fibers aligned with the direction of the ply drops. The fiber orientation influences the permeability of the laminate and affect the flow of resin to low pressure regions. Two laminate thicknesses were studied to interrogate the effect of consolidation on driving resin flow to low pressure regions.

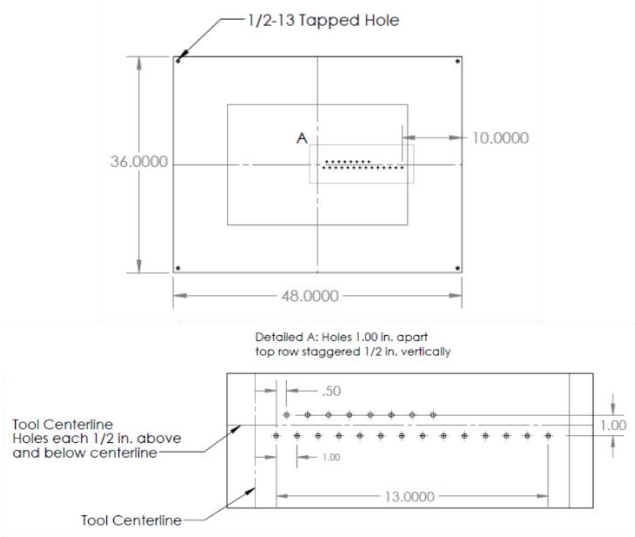

Figure 4: Schematic of tool and sensor locations.

Table 1. Test plan for local resin pressure evaluation

Test ID	Caul Thickness (in)	Layup	No. of plies dropped (every ½ in)	Edge Dam	Autoclave Pressure	Number of plies in the thick region
1 (Baseline)	0.5 (12.7 mm)	Quasi-isotropic	2	Yes	85 psi (103 kPa)	32 plies
2	0.125 (3.2 mm)	Quasi-isotropic	2	Yes	85 psi (103 kPa)	32 plies
4	0.5 (12.7 mm)	Unidirectional	2	Yes	85 psi (103 kPa)	32 plies
5	No caul	Quasi-isotropic	2	Yes	85 psi (103 kPa)	32 plies
6	0.5 (12.7 mm)	Quasi-isotropic	3	Yes	85 psi (103 kPa)	40 plies

Cure cycle:
Vacuum of 15 psig (103 kPa) and autoclave of 85 (586 kPa) psig applied
Vent vacuum when pressure reaches 30 psig
Heat to 107 °C at 2 °C/min
Hold for 30 min
Heat to 176 °C at 2 °C/min
Hold for 240 min
Cool at 3 °C/min to room temperature and vent pressure

Sensors were embedded in the tool to capture the linear profile along the ply drops at a resolution of ½ inch spacing. The panel was sealed around the perimeter with breaker tape to prevent resin bleed and promote a pseudo-1D resin flow problem from the center of the laminate towards the thin regions at the ends. Each sensor was calibrated in the temperature range of 22 to 100 °C at incremental pressure values of 0, 14, 45, and 85 psi (0, 96, 310, 103 kPa), to convert the voltage reading into pressure. An image of a sensor is shown below in Figure 5. The dependency of the sensors on temperature has been studied and an approximate error of ± 2 psi (±13.8 kPa) was observed. Two thermocouples were placed in the middle of the sensor array on the tool and averaged for the calibration of the sensors. Thermocouple data were collected between the panel and the tooling in the center of the sensors to have an accurate reading of the temperature near the sensors for the conversion into pressure.

Figure 5. Image of the resin pressure sensor.

2.2 Experimental Resin Pressure Results

Local resin pressure has been evaluated with respect to location and time in order to observe trends between each test. The resin pressure data measured was most meaningful during the early stages of the cure cycle when viscosity began to decrease and in the low viscosity regions. Beyond

gelation, the data from the sensors was not representative of resin flow but reflected more complex phenomena. Figure 6 shows the resin pressure profile along the part for each test at minimum viscosity (based on 8552 material model). The effect of the thick caul sheets (0.5 in, 12.7 mm.) was clearly visible in tests 1, 4, and 6 where the pressure built away from the center of the laminate towards the ply drops. At approximately 5.5 in. (0.14 m) the resin pressure peaks due to the stress concentration of the caul sheet on the corner where ply drops began. Continuing to move down the ply drops, the pressure decreased as the caul sheet minimizes the pressure seen in the laminate. This response was not seen in the thin caul sheet (test 2) or the no caul test (test 5). The pressure in the test with no caul sheet was uniform as the bag allowed pressure to be applied evenly to the surface even with non-uniform thicknesses. The thin caul was more flexible allowing it to conform to the ply drops and apply pressure evenly over the laminate. However, the spike in the pressure at the end the laminate in test 2 was reflective of the end of the caul bending into the laminate. Small differences were also observed between test 4 (unidirectional lay-up) and tests 1 and 6 (quasi-isotropic lay-up) which all used a thick caul sheet. The change in permeability due to the fiber orientation was expected to influence resin flow and measured resin pressure between the two configurations. Ultimately, if these trends can be captured in simulation and traced to local void formation and porosity, a tool for predicting final porosity can be developed.

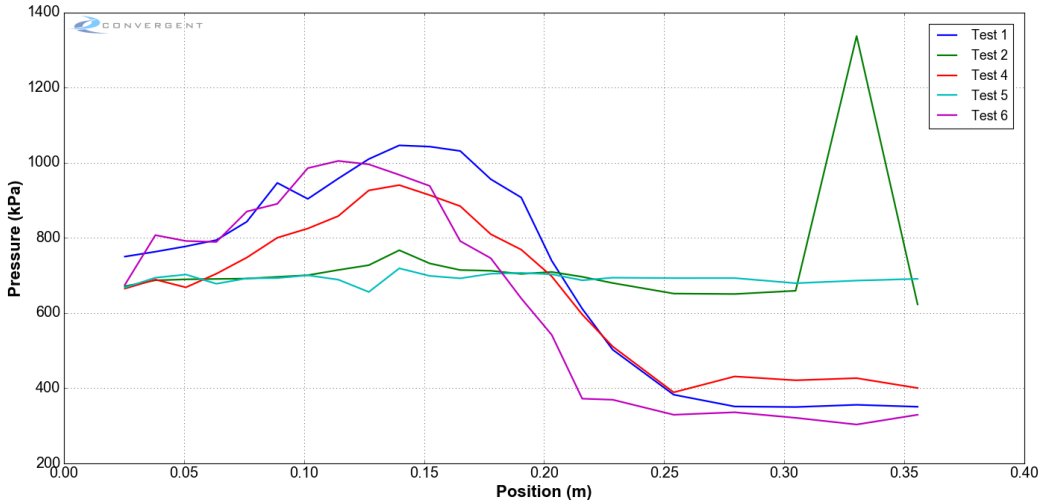

Figure 6. Resin pressure along the ply drop profile at minimum viscosity.

Data from sensors 10 and 18 have been extracted and plotted below with respect to time in Figure 7 and Figure 8. These two positions represented locations either near the beginning of the ply drops (sensor 10) or near the end of the tapered region (sensor 18). Tests 2 and 5 had a uniform pressure profiles over the early stages of the cure cycle. The flexible caul sheet, or no caul sheet allowed a uniform pressure to be applied leading to no large pressure gradients to drive resin flow. Tests 1, 4, and 6 showed similar trends, due to the thick caul sheet, but there were shifts in the timing when pressure begins to drop. Overall, a pressure gradient was expected moving from the thick region towards the thin region of the laminate. A pressure drop was measured in the thick region as resin flowed away, and pressure subsequently increased in the thin region as resin flowed in. The two regions did not equilibrate because the thick caul sheet concentrated pressure from the autoclave on the thick region of the laminate. The higher permeability in unidirectional laminate (test 4) promoted the flow of resin as demonstrated by the response time in both figures. We noted that the general

response of the pressure histories in terms of location and timing was consistent with the previous work by Roy [16].

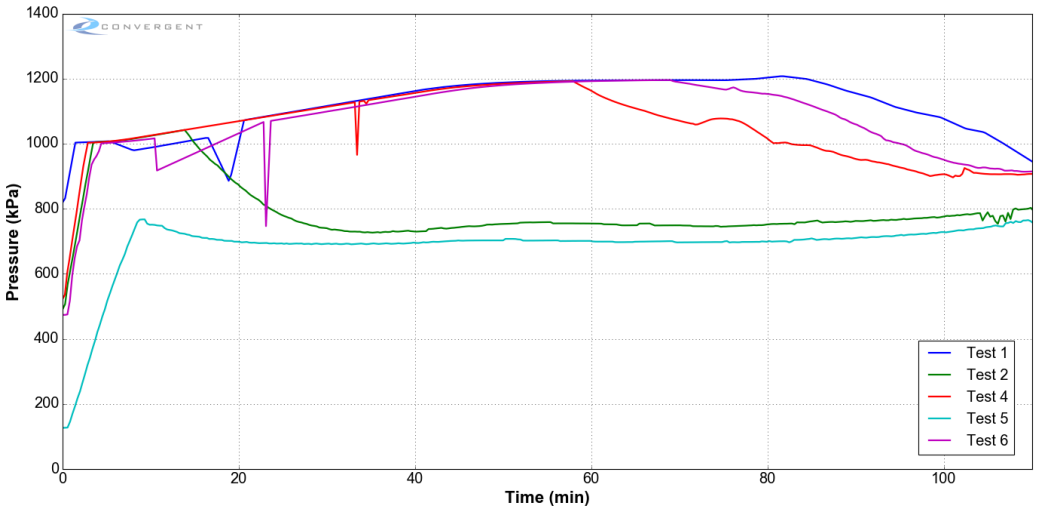

Figure 7. Comparison of Sensor 10 resin pressure in tests 1, 2, 4, 5, and 6.

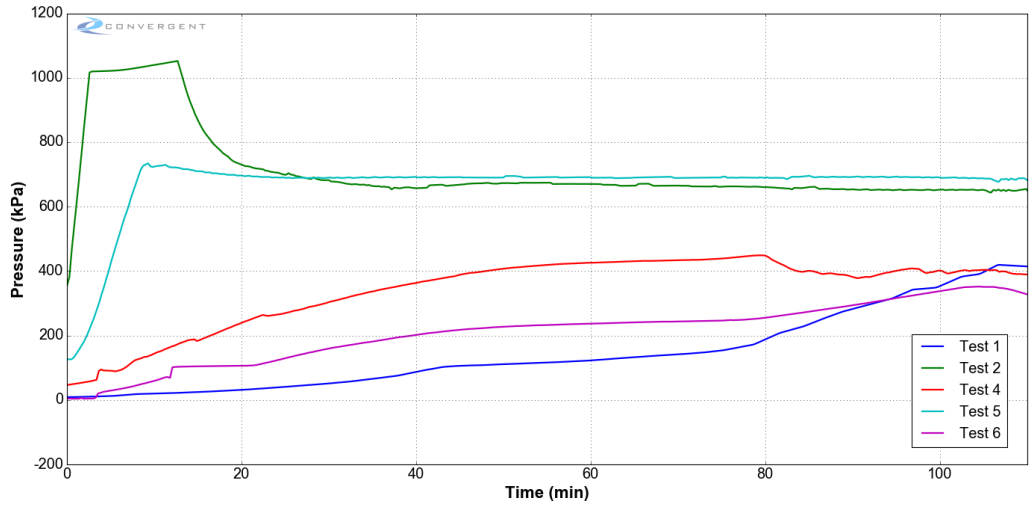

Figure 8. Comparison of Sensor 18 resin pressure in tests 1, 2, 4, 5, and 6.

3. NUMERICAL SIMULATIONS

The numerical simulation in this study was performed using COMPRO-ANSYS. The material model used in this study was Hexcel AS4/8552 as currently there is no completed model for Hexcel IM7/8552-1. The material model included a viscosity model and compaction model which updated with time, temperature and degree of cure. This model had the capability of predicting the local resin viscosity due to temperature and degree of cure which updated the local resin pressure and resin flow through the fiber bed. The material model response is shown below in Figure 9 for degree of cure and viscosity with the defined cure cycle.

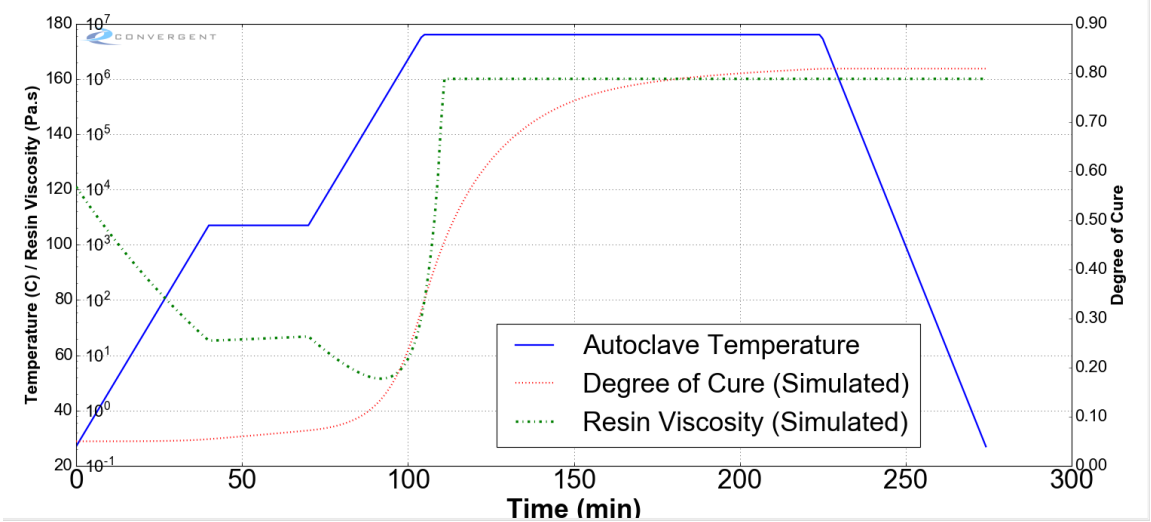

Figure 9: Applied temperature profile and resin viscosity.

These simulations did not include a thermal analysis, and assumed a uniform temperature profile that matches the thermocouple (TC) data. In these simulations, temperature was uniformly applied as a boundary condition to the part and caul sheet. This assumption may cause discrepancies between the simulation and test results. Figure 10 and Figure 11 show the model geometry as application of applied pressure in the two different tests (0.5 inch caul and no caul) as described in Table 1. Due to symmetry, only half of the geometry was simulated.

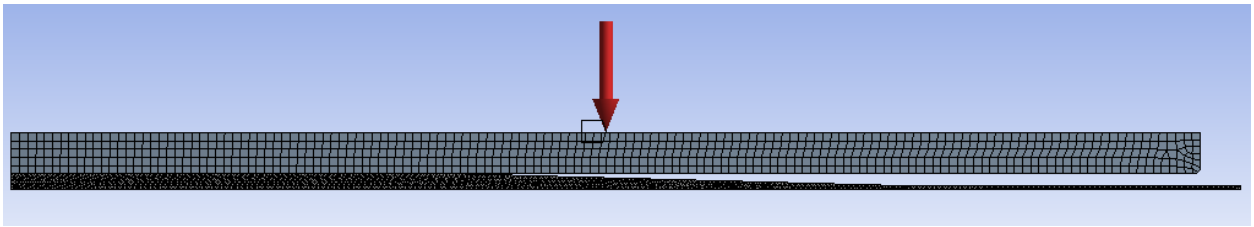

Figure 10: Applied autoclave pressure as mechanical pressure BC on top of the caul in test ID-1 (0.5-inch-thick caul).

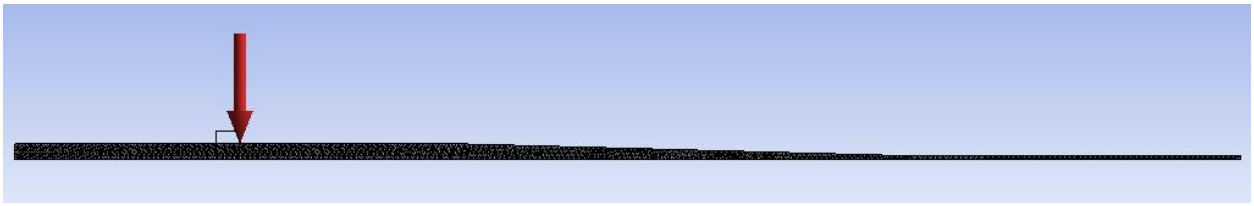

Figure 11: Applied autoclave pressure as mechanical pressure BC on top of the part in test ID-5 (no caul).

Figure 12 shows the resin pressure versus time for 5 different resin pressure locations (RP1, RP4, RP10, RP15, and RP20) for test ID5 (no caul). As expected, in the absence of a caul there was uniform resin pressure in the part resulting in minimum resin displacement.

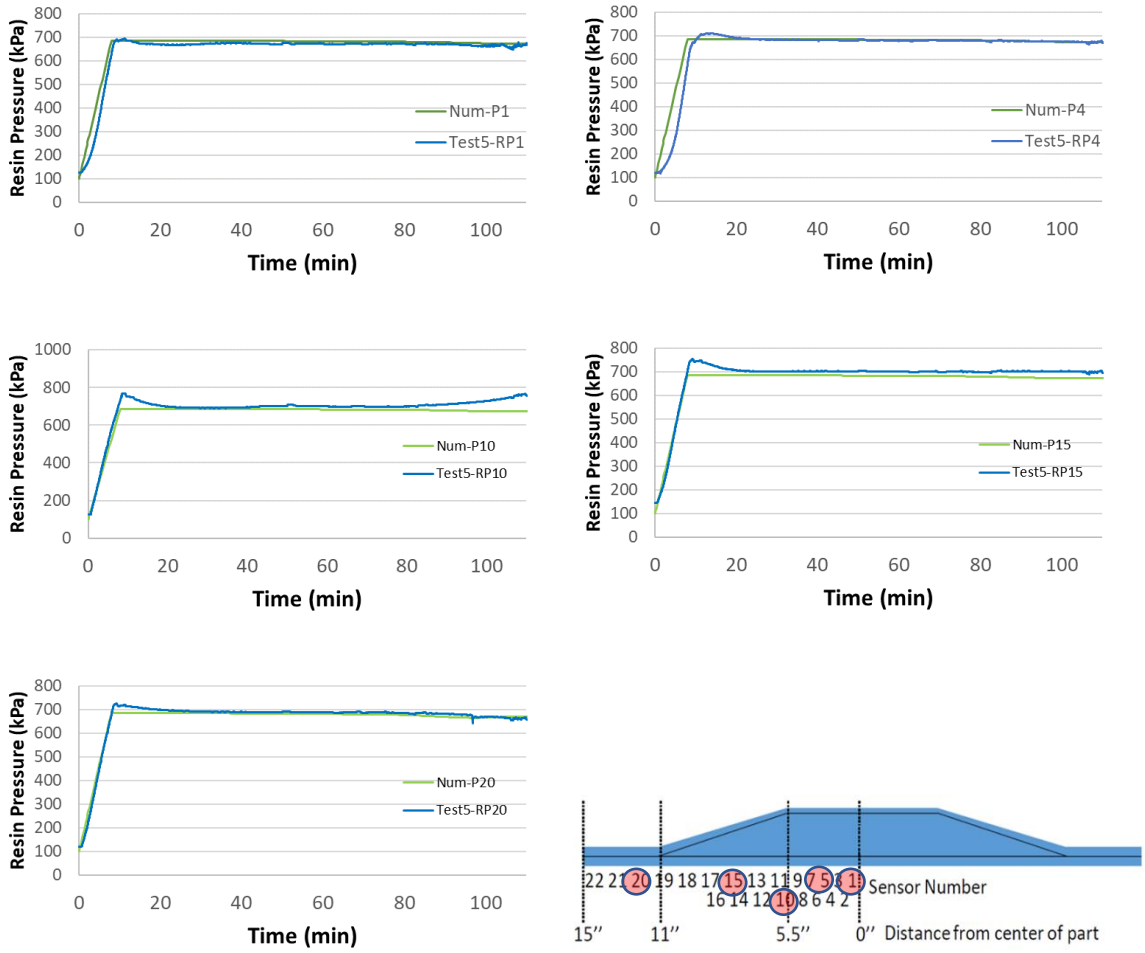

Figure 12: Comparison of resin pressure in simulation and experimental data in test ID 5 (no caul).

4. CONCLUSIONS

In this study, a framework for calculation of resin pressure in the formations has been developed and preliminary validation performed. The Integrated Flow Stress 3 Phase (IFS3P) framework has been simplified by assuming that the gas and the resin share the same pressure, thus enabling implementation in available COTS general purpose software for numerical simulations.

A series of composite parts and caul plates were manufactured and processing trials conducted to measure resin pressure under a variety of layup and bagging configurations. In the case of the thicker caul plate, the lack of compliance to the laminate surface leads to a non-uniform distribution of pressure causing high and low-pressure points.

This study shows how a three-phase compaction simulation, even when simplified, can provide information about resin pressure history and pressure distribution in parts with geometric features.

5. ACKNOWLEDGMENTS

The authors would like to thank Prashant Khare, Ankur Jaura, and Dinesh Kumar of ANSYS Inc for their support in development of COMPRO-ANSYS. This work was partially performed under the sponsorship of the National Aeronautics and Space Administration under NASA Project ID: NNL16AA09C.

6. REFERENCES

[1] H. Bedayat *et al.*, "An Efficient Modelling Approach for Prediction of Porosity Severity in Composite Structures," in *SAMPE International Symposium*, 2017.

[2] M. Roy, J. Kay, G. Fernlund, and A. Poursartip, "Porosity in Configured Structures," *Proc. SAMPE Tech. Conf. Balt. Maryl. May 18-21*, p. 15, 2015.

[3] L. Farhang, "Void evolution during processing of out-of-autoclave prepreg laminates," The University of British Columbia, 2014.

[4] K. Terzaghi, "Erdbaumechanik auf bodenphysikalischen Grundlagen," *Wien Deuticke*, 1925.

[5] M. A. Biot and D. G. Willis, "The elastic coefficents of the theory of consolidation," *J. Appl. Mech.*, vol. 24, pp. 594–601, Jan. 1957.

[6] J. R. Rice and M. P. Cleary, "Some basic stress diffusion solutions for fluid-saturated elastic porous media with compressible constituents," *Rev. Geophys.*, vol. 14, no. 2, p. 227, 1976.

[7] M. A. Biot, "General theory of three-dimensional consolidation," *J. Appl. Phys.*, vol. 12, no. 2, p. 155, 1941.

[8] S. Amini Niaki, "A three-phase integrated flow-stress framework for process modelling of composite materials," The University of British Columbia, 2017.

[9] P. Hubert, "Aspects of flow and compaction of laminated composite shapes during cure," The University of British Columbia, 1996.

[10] P. Hubert, R. Vaziri, and A. Poursartip, "A two-dimensional flow model for the process simulation of complex shape composite laminates," *Int. J. Numer. Methods Eng.*, vol. 44, no. 1, pp. 1–26, Jan. 1999.

[11] S. M. Haghshenas, "Integrating resin flow and stress development in process modeling of thermoset composites," The University of British Columbia, 2012.

[12] R. Lewis and B. Schrefler, *Finite Element Method in the Deformation and Consolidation of Porous Media*. 1998.

[13] S. A. Niaki, A. Forghani, R. Vaziri, and A. Poursartip, "A two-phase integrated flow-stress process model for composites with application to highly compressible phases," *Mech. Mater.*, vol. 109, pp. 51–66, 2017.

[14] S. A. Niaki, A. Forghani, R. Vaziri, and A. Poursartip, "A three-phase integrated flow-stress model for processing of composites," *Submitt. to Mech. Mater.*, 2017.

[15] Convergent, “COMPRO.” Vancouver, BC, Canada, 2017.

[16] M. Roy, “Porosity in configured structures : effect of ply drops and caul sheets in the processing of composite parts,” University of British Columbia, 2015.